Molecular Dynamics Study of Unbinding of the Avidin-Biotin Complex

S. Izrailev, S. Stepaniants, M. Balsera, Y. Oono, and K. Schulten
Beckman Institute and Department of Physics, University of Illinois, Urbana, Illinois 61801 USA

ABSTRACT We report molecular dynamics simulations that induce, over periods of 40–500 ps, the unbinding of biotin from avidin by means of external harmonic forces with force constants close to those of AFM cantilevers. The applied forces are sufficiently large to reduce the overall binding energy enough to yield unbinding within the measurement time. Our study complements earlier work on biotin-streptavidin that employed a much larger harmonic force constant. The simulations reveal a variety of unbinding pathways, the role of key residues contributing to adhesion as well as the spatial range over which avidin binds biotin. In contrast to the previous studies, the calculated rupture forces exceed by far those observed. We demonstrate, in the framework of models expressed in terms of one-dimensional Langevin equations with a schematic binding potential, the associated Smoluchowski equations, and the theory of first passage times, that picosecond to nanosecond simulation of ligand unbinding requires such strong forces that the resulting protein-ligand motion proceeds far from the thermally activated regime of millisecond AFM experiments, and that simulated unbinding cannot be readily extrapolated to the experimentally observed rupture.

INTRODUCTION

Binding and unbinding of ligands to proteins is an essential biochemical process, and the underlying mechanisms must be known for an understanding of enzyme reactions (Kuby, 1991), the recognition of ligands by their receptors (Conn, 1993) or of DNA sequences by regulatory proteins (Schwabe et al., 1993), and for the design of drugs. These processes have in common a transition from one equilibrium state to another, which often is a rare event on the picosecond to nanosecond time scale of molecular dynamics (MD) simulations. To characterize rare events through molecular dynamics simulation, one can add external forces that reduce energy barriers and speed up the kinetics. This approach corresponds closely to micromanipulation through atomic force microscopy (AFM) (Binning et al., 1986) or optical tweezers (Block and Svoboda, 1994) and promises to develop into a major modeling tool for the exploration of reaction pathways, in particular, because simulations of biopolymer systems with up 1000 atoms can now be achieved interactively by using new software packages (Nelson et al., 1995).

An important step toward understanding of binding and unbinding mechanisms has been achieved by Grubmüller, Heymann and Tavan (1996) who simulated the unbinding of the streptavidin-biotin complex. In a set of pioneering simulations these authors equilibrated a streptavidin monomer with bound biotin in a bath of water molecules and exerted forces that led to unbinding. Carrying out computationally extensive simulations on a parallel computer, the authors were able to slow down the simulated unbinding to one nanosecond. However, this is many orders of magnitude faster than natural reactions and such rapid unbinding is necessarily accompanied by extreme irreversible work; the latter is expended in addition to the work required by the thermodynamic potentials. The irreversible work may be determined by monitoring the increase of temperature, hysteresis, or otherwise, and discounted to reveal the thermodynamic potential. The prevailing attitude in simulations is to strive for the ideal of reversibility, e.g., in free energy perturbation theory (McCammon and Harvey, 1987), which requires extremely slow manipulation and is often impossible to achieve. However, unbinding of substrates and the breaking of the adhesion linkages of biopolymers involve nonequilibrium processes. It is known that the work required to sever an adhesive bond in industrial adhesives has a large irreversible component that can be orders of magnitude larger than the work required by the underlying thermodynamic potentials (Baljon and Robbins, 1996). One expects that noncovalent (i.e., adhesive) linkages in biological cells (Evans et al., 1995) gain their strength similarly from nonequilibrium properties. Because biological processes occur more or less far from equilibrium and, therefore, involve irreversible contributions, one may actually consider the rapidity of simulated ligand unbinding an advantage rather than a disadvantage, as long as one can estimate the irreversible work involved with satisfactory accuracy.

Nevertheless, two questions arise: To what extent does fast unbinding, induced on the picosecond to nanosecond time scale of molecular dynamics simulations, relate to the natural mode of dissociation, and can it be extrapolated to the time scales of AFM experiments? Both in AFM experiments and in computer simulations, the barrier of unbinding is lowered by the application of an external force. If the applied force is not large enough to eliminate the barriers, the unbinding can still be induced by thermal fluctuations at

Received for publication 18 September 1996 and in final form 5 December 1996.

Address reprint requests to Dr. Klaus Schulten, Department of Physics, Beckman Institute 3147, University of Illinois, 405 N. Mathews Ave., Urbana, IL 61801. Tel.: 217-244-2212; Fax: 217-244-6078; E-mail: kschulte@ks.uiuc.edu.

0006-3495/97/04/1568/14 $2.00

a larger rate than without external forces. Thermal fluctuations should also govern the dissociation of biotin from avidin in AFM experiments lasting a few milliseconds (Evans and Ritchie, 1996). The rupture force measured in such experiments is defined as the largest force applied during the unbinding. In the case in which the AFM experiments were arbitrarily slow, the rupture force would actually measure zero, because any barrier can be thermally overcome if one waits long enough.

Let us assume for the sake of argument that external forces overwhelm all barriers, so that the motion of the ligand can be characterized as free diffusion with a diffusion coefficient of 1 $Å^2$/ns. The latter coefficient is suggested by Mößbauer line shape measurements sampling the motion of the heme in myoglobin over 100 ns (Nadler and Schulten, 1984). Unbinding that involves ligand motion over a range of about 10 Å then requires 10–100 ns (i.e., even a barrierless rupture could not be sampled by molecular dynamics simulations covering only shorter time scales). For such simulations to induce rupture, extremely strong forces that overcompensate barriers must be applied. In this case the ligand is subject to a drift rather than diffusive motion in which neither barriers nor thermal forces contribute significantly. This regime is clearly different from that of thermally activated processes governing millisecond AFM experiments, in which barriers of about 10 kcal/mol can be surmounted spontaneously.

A proper interpretation of AFM experiments must account for the functional form of the applied force, e.g., if the ligand is pulled with a stiff or with a weak elastic spring. What matters is the width δx of thermal (temperature T) motion related to the spring constant f through $\delta x = (k_B T/f)^{1/2}$. AFM cantilevers have spring constants that confine the motion of ligands within 3-Å sampling regions, which is a size comparable to the length of the binding pockets. Grubmüller et al. (1996) employed a spring with $\delta x = 0.4$ Å, which samples only local forces. It is desirable to investigate ligand unbinding, using for the manipulation of unbinding spring constants close to those of AFM cantilevers.

Accordingly, we investigate in this paper the fast mechanical manipulation of protein-ligand systems using soft springs. We focus on the protein avidin and its ligand biotin. We introduce the simulation methods, compare the results of simulations to AFM experiments, and establish a conceptual basis for enforced ligand unbinding through consideration of models that are expressed in terms of one-dimensional Langevin equations with simple potential energy functions, associated Smoluchowski equations (Gardiner, 1985), and the theory of first passage times (Schulten et al., 1981; Nadler and Schulten, 1985).

The protein considered in our study, avidin isolated from hen egg white (Heney and Orr, 1981), is a tetrameric glycoprotein consisting of 512 amino acid residues and composed of almost 8000 atoms. Biotin is a 32-atom vitamin (see Fig. 1) that functions as an activated CO_2 carrier in some biochemical reactions (e.g., in the carboxylation of pyruvirate). Because of its tetrameric structure, avidin can

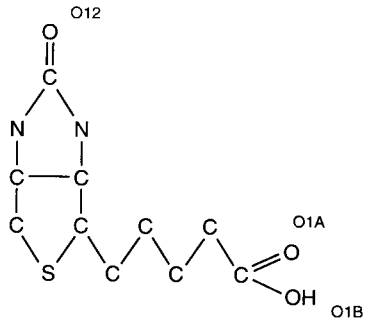

FIGURE 1 Chemical structure of biotin.

bind up to four molecules of biotin. The binding affinity is extremely high, characterized through a Helmholtz free energy and enthalpy change of about 20 kcal/mol (Suurkusk and Wadso, 1972; Swamy, 1995; Miyamoto and Kollman, 1993) and a binding constant of $K_d = 10^{-15}$ (Green, 1975). This makes the avidin-biotin system an excellent tool in various types of experiments, for example, in affinity cytochemistry, affinity chromatography, diagnostics, biosensors, targeted drug delivery (Bayer and Wilcheck, 1980; Wilcheck and Bayer, 1989; Green, 1990), and immunoassays (Kanzaki and Iwasawa, 1995). As in other high-affinity systems, the unusually slow dissociation kinetics (Balgi et al., 1995) of the protein-ligand complex is governed by an exceptionally tight binding between protein and ligand.

Despite the numerous experimental applications and therapeutic importance of avidin for medicine, the unusually high affinity and mechanism of adhesion of avidin to biotin had not been thoroughly investigated until the three-dimensional structure of avidin at 2.7-Å resolution was reported recently (Livnah et al., 1993; Pugliese et al., 1993, 1994). The structure revealed that each monomer has an eight-stranded, antiparallel orthogonal β-barrel with extended loop regions. Avidin binds biotin strongly through interactions with polar and aromatic residues of the binding site, which is presented in Fig. 2.

Measurements of molecular interactions requiring high precision and spatial resolution are furnished by magnetic force experiments (Wang et al., 1993), pipette suction experiments (Evans et al., 1991), experiments with a surface force apparatus (Leckband et al., 1994; Israelachvili, 1992), and optical tweezers (Svoboda and Block, 1994). The AFM technique had recently been applied to measure the adhesion force between avidin and biotin. For this purpose the tip of the atomic force microscope cantilever was derivatized with avidin and agarose beads functionalized with biotin (Florin et al., 1994; Moy et al., 1994a,b). The measurement is presented schematically in Fig. 3. The resulting force value was found to be 160 ± 20 pN (Florin et al., 1994; Moy et al., 1994b). The separation of the tip from the bead was attributed to the release of biotins connected to the AFM tip from their binding pockets in avidin.

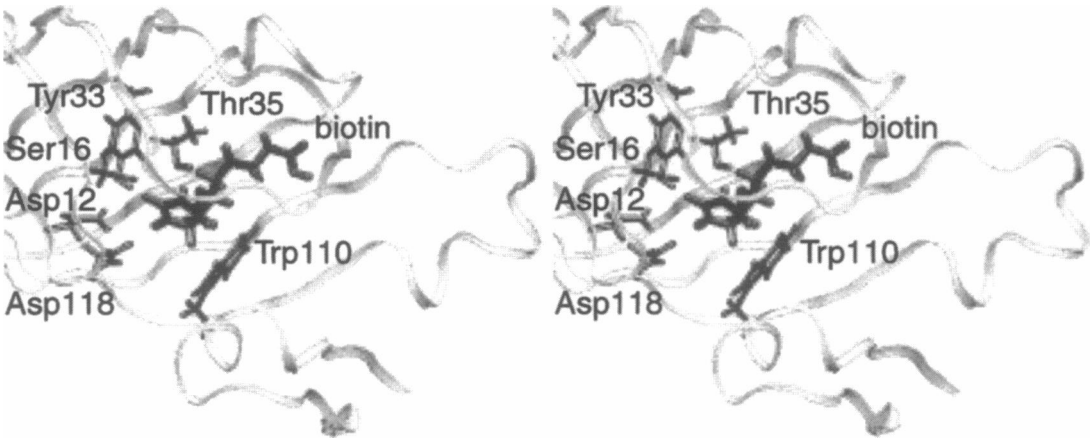

FIGURE 2 Biotin binding pocket. Stereo image of the biotin binding in avidin. Shown are the main amino acid side groups that make contacts with biotin along the rupture paths.

METHOD

MD simulations of the avidin-biotin complex were carried out using the program X-PLOR (Brünger, 1992) with version 22 of the CHARMM (Brooks et al., 1983) force field. We constructed an avidin tetramer from crystallographic symmetry based on the atomic coordinates of the reported dimer structure (Livnah et al., 1993; Pugliese et al., 1993, 1994), entry 1AVD in the Brookhaven Protein Data Bank (Bernstein et al., 1977).

It has been argued that the binding pocket of avidin is inaccessible to water (Pugliese et al., 1993). We tested this supposition in an attempt to place water in the binding pocket with the modeling package DOWSER (Zhang and Hermans, 1996). Indeed, we found that the tight contact between biotin and the binding pocket makes it unlikely for more than one water molecule to fit inside the binding pocket. We chose, hence, not to introduce water into the binding pocket in our simulations, having possibly missed a single water. Alternatively, one might carry out simulations placing at each moment in time the maximum number of internal waters into the binding pocket, accounting, thereby, for water penetrating into the binding pocket on a slower time scale than that covered by the actual simulation.

A charge distribution for biotin was obtained by means of the program GAUSSIAN-94 (Frisch et al., 1995) at the Hartree-Fock level with a 6–31G* basis set, using the coordinates of heavy atoms taken from the crystal structure (chain B from entry 1AVD in the Protein Data Bank) and of hydrogens generated by the program QUANTA (MSI, 1994). The equilibrium bond length, angles, torsional angles, and force constants for biotin were derived from biotin coordinates and force-field parameters of molecules with similar chemical structure available in CHARMM and X-PLOR (the topology and parameter files for biotin are available via anonymous ftp at ftp://ftp.ks.uiuc.edu/ in directory /pub/projects/biotin).

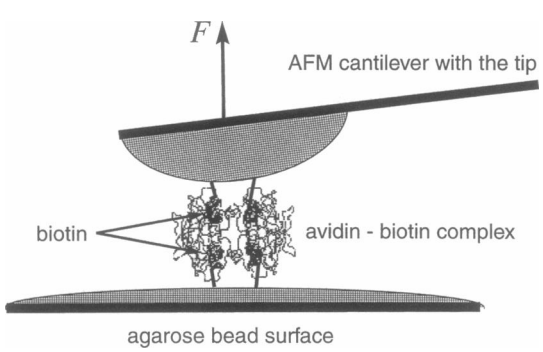

FIGURE 3 Schematic representation of atomic force microscopy (AFM) experiment on the avidin-biotin complex. An AFM tip attached to an elastic cantilever is linked to biotin; the agarose bead surface is linked chemically to biotin through stiff bonds; an avidin tetramer binds to two biotins on the bead and to two biotins connected with the AFM tip; the cantilever applies forces measured by monitoring the position of the tip.

In all simulations we assumed a dielectric constant $\epsilon = 1$ and a cutoff of Coulomb forces with a switching function starting at 10.7 Å and reaching zero at a distance of 14.3 Å. All atoms, including hydrogens, were described explicitly. The hydrogen atom coordinates of both avidin and biotin were generated using the HBUILD routine of X-PLOR. An integration time step of 1 fs was employed. The avidin tetramer structure was energy minimized and allowed to equilibrate in a 45-ps molecular dynamics run.

To facilitate the exit of biotin from its binding pocket, we altered the conformation of the 3-4 loop (residues 35–46) (Pugliese et al., 1993) of avidin, which almost completely closes the pocket, but can fluctuate to an open conformation on the time scale of the AFM experiment. The new conformation of the loop was achieved using MDScope (Nelson et al., 1995), which includes the molecular graphics program VMD (Humphrey et al., 1996) connected to the molecular dynamics program NAMD (Nelson et al., 1996), the latter running on a workstation cluster. VMD allowed us to monitor and control the simulation of the avidin-biotin complex and to interactively apply forces to selected atoms on the 3-4 loop of one of the avidin monomers. The forces were sent from VMD to NAMD and introduced into the molecular dynamics simulations. The application of the external forces to the system led to the desired conformational change of the loop (see Fig. 4). This procedure was followed by a 15-ps equilibration. The resulting structure served as the starting point of each simulation reported here, in which the C_α atoms of the loop residues were constrained to prevent a renewed closure of the binding pocket.

External forces were applied to the tail of one of four biotins through the definition of harmonic restraints in X-PLOR. One of the oxygen atoms of biotin's valeryl side-chain carboxylate group was restrained to a point outside the binding site at a distance of 20 Å, i.e., far enough to ensure that biotin at the point of restraint would be completely outside the pocket. The position of the restraint point was chosen so that biotin would encounter the least hindrance when moving from its initial position toward the point of restraint, a direction that is assumed to represent the orientation of the force applied by the AFM tip.

The absolute value of the force acting on biotin was chosen to be

$$|F| = k(t)d, \tag{1}$$

where k is the harmonic restraint coefficient that can be specified in X-PLOR, and where d is the distance between the tail of biotin and the

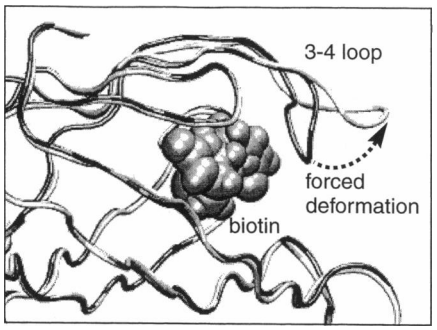

FIGURE 4 Forced conformational change of the 3-4 loop of the avidin monomer. The structures of the monomer before and after the change are superimposed.

point of restraint. The coefficient k was linearly increased every 100 fs with a rate α as described by

$$k(t) = \alpha t, \tag{2}$$

starting at $t = 0$, i.e., with a vanishing force. In the simulations we monitored the ensuing motion of biotin, focusing mainly on the coordinate $x(t)$ of the center of biotin along an axis given by the line connecting the initial ($t = 0$) position of biotin's center with the point of restraint.

Eight simulations were performed for the rate α covering a span of almost two orders of magnitude, namely, $\alpha = 100, 50, 20, 10, 8, 5, 4, 2 \times 10^{-3}\ k_BT$/ps Å^2, where $k_BT \simeq 0.6$ kcal/mol $\simeq 41.4$ pN Å. This range of α allowed us to explore how the unbinding of biotin depends on the speed of rupture. Ideally one would choose α in accordance with experiments, e.g., such that the rupture occurs on a millisecond time scale; however, respective simulations are infeasible. In fact, the simulations carried out for the present situation required, on a Hewlett-Packard 735/125 workstation, about 2 h/ps, such that only time scales of a few hundred picoseconds could be covered.

To prohibit rotation and translation of the entire tetramer due to the force applied to biotin, the tetramer had to be constrained at three separate points. We selected for this purpose the centers of three of the four monomers. These centers were restrained to their initial positions using a harmonic potential with a coefficient $k = 600$ kcal/mol Å^2 (cf. Eq. 1).

RESULTS

To simulate the rupture of biotin from its binding site, the time-dependent forces defined through Eqs. 1 and 2 were applied for eight choices of the rate α. We monitored the position x of biotin, the applied force, the distances between biotin and the polar residues inside the binding pocket, as well as the interaction energies between biotin and key residues in the pocket.

The analysis of these data along with visual observations using VMD (Humphrey et al., 1996) showed that the motion of biotin inside the binding pocket develops in a series of slips. Between two consecutive slips biotin is dragged toward the opening of the binding pocket. The motion due to the drag is nearly invisible for the short (large α) trajectories and becomes more discernible for the long (small α) trajectories. Each slip can be identified with the breakage of a network of bonds that biotin forms with polar residues inside the pocket.

Between two consecutive slips, the dragging of biotin produces only small displacements such that the applied force grows linearly until it is sufficiently large to break the network of hydrogen bonds. Once the bonds are broken, biotin slips along the pocket. The latter leads to a rapid contraction of the distance d between the tail of biotin and the point of restraint and, therefore, to a significant decrease in the applied force according to Eq. 1. Such a momentary decrease can arise even though the force constant $k(t)$ is monotonously increased in time according to Eq. 2.

The onward slip of biotin is terminated once biotin sticks to another set of polar residues in the pocket. The force, significantly reduced because of the contraction of the distance d, must increase again to induce a new rupture. The motion of biotin thus occurs in discrete steps and represents sequences of dragging, slipping, and sticking produced by the action of the extruding force.

The behavior of biotin is depicted in Figs. 5–8 for the rate $\alpha = 0.002 k_BT$/ps Å^2. The presentation of the position $x(t)$ of biotin relative to the binding pocket in Fig. 5 *b* reveals the moments when biotin slips from one position inside the binding pocket to another. Between the slips biotin is nearly at rest, as indicated by plateau-like regions of $x(t)$. One can

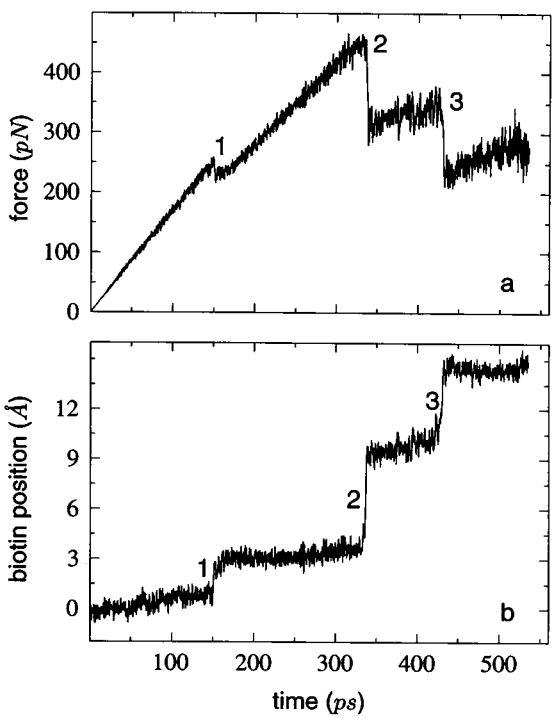

FIGURE 5 (*a*) Force applied to the tail of biotin as a function of time. While biotin is nearly at rest, the force grows linearly until the moment of a slip, when a network of hydrogen bonds breaks and another one forms. (*b*) Position of the geometric center of biotin as a function of time. Plateaus on the plot correspond to the positions of biotin between the slips (see also Fig. 7). Numbers 1–3 on the plots correspond to the moments of the slips (see Table 1 for details).

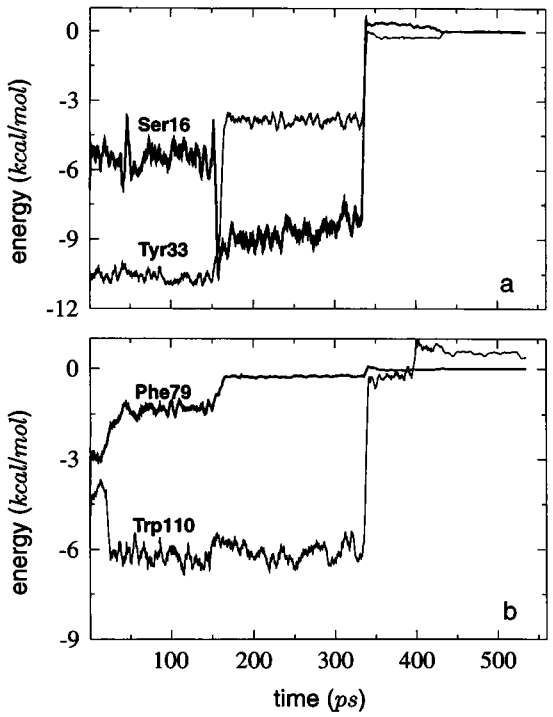

FIGURE 6 (*a*) Energies of interaction of Tyr33 and Ser16 with biotin. After the breakage of the bond with Tyr33 (abrupt increase in interaction energy), biotin moves closer to Ser16 (abrupt fall in interaction energy). (*b*) Energies of interaction of Trp110 and Phe79 with biotin. First, biotin moves away from Phe79 (increase in interaction energy) to Trp110 (fall in interaction energy). Then biotin leaves the binding pocket and loses its contact with Trp110 (increase in interaction energy).

discern that biotin fluctuates around its original position for 150 ps until the applied force is sufficient to move it abruptly to a new position, 3 Å away from the origin. Here biotin remains for 190 ps until it slips to a position located 9 Å from the origin. This slip is associated with unbinding, and the applied maximum force (450 pN in this case; see Fig. 5 *a*) is termed the rupture force. The total displacement of biotin of about 8 ± 1 Å, immediately after a slip, is consistent throughout all simulations and is close to the size of the binding pocket (Pugliese et al., 1993). Once out of the binding pocket, the head of biotin, i.e., its ureidic and tetrahydrothiophenic rings, adheres to the residues outside the binding pocket, including those on the 3-4 loop of avidin. A series of subsequent plateaus corresponding to these adhesions are seen in Fig. 5 *b* to begin at 340 ps and 430 ps.

To elucidate the mechanism of rupture we analyzed the interaction energies along with the distances between biotin and different residues in the binding pocket. Our analysis shows pronounced jumps in the energies of interaction of biotin with the polar residues Asn12, Ser16, Tyr33, Thr35, and Asn118, which strongly contribute to the adhesion of the head of biotin to the bottom of the binding pocket. The strongest bonds are formed between Asn12, Ser16, Tyr33, Thr35, and ureido oxygen and nitrogens of biotin. The breakage of bonds with Tyr33 and Asn12 is accompanied by the jump of the interaction energies by about 10 kcal/mol and 8 kcal/mol, respectively. The effect of Asn118 is relatively weak (contributing about 3 kcal/mol). The rupture of the bond with Asn118 is followed by the rupture of the bonds with Asn12 and Tyr33, which subsequently allows biotin to move closer to Thr35 and Ser16. New hydrogen bonds, identified by a sharp fall in biotin's interaction energy with Thr35 and Ser16, are formed between biotin and the latter residues. These hydrogen bonds involve the interactions of ureido oxygen and nitrogen of biotin with Thr35 and Ser16. Examples of the time development of the interaction energies are presented in Fig. 6.

Aromatic residues Trp70, Trp97, Phe79, and Trp110 surround biotin in the binding pocket. The role of these residues is crucial in the unbinding process. The detachment of the head of biotin from Phe79 and Trp97 is accompanied by an increase in the interaction energy (by about 3 kcal/mol and 5 kcal/mol, respectively) and happens in the beginning of the unbinding pathway. The increase in the interaction energy with Trp110 and Trp70 (about 6 kcal/mol and 5 kcal/mol, respectively) takes place at a later time, which indicates that during the process of unbinding biotin maintains a continuous contact with these residues (see Fig. 6 *b*).

The snapshots of polar and nonpolar contacts of biotin during its stepwize motion out of the binding pocket are shown in Figs. 7 and 8 and correspond to the plateaus seen in Fig. 5 *b*. The presented trajectory captures the essential details of biotin unbinding, although one must note that separate trajectories exhibit significant differences among their respective unbinding pathways. The variation of the pathways is documented in Table 1.

Table 1 represents variations in the unbinding pathways of biotin for various trajectories. For the sake of simplicity, we present only polar contacts of the biotin head with the residues inside the binding pocket. Numbers in the top correspond to the numbering of the slips in Fig. 5, *a* and *b*. The residues with which biotin loses contact are specified in the upper row in each cell; the residues in the lower row are the ones with which biotin forms new contacts. The leftmost vertical column contains the parameter α of the respective simulations; the rightmost column contains the respective values of the rupture forces. Because we are mainly interested in slips of biotin before exit from the binding site, we did not include in Table 1 contacts that the biotin head makes outside the binding site. The actual unbinding pathway of biotin is more intricate than could be presented in Table 1.

The disagreement between the numerical values in the unbinding forces of our simulations and those measured in AFM experiments may seem disappointing. In the next section we show that these discrepancies are the inevitable consequence of the different time scales on which the unbinding is enforced in MD and AFM experiments. For this purpose, we introduce models, based on one-dimensional motion in the strong friction limit, that capture the esssence of the unbinding processes.

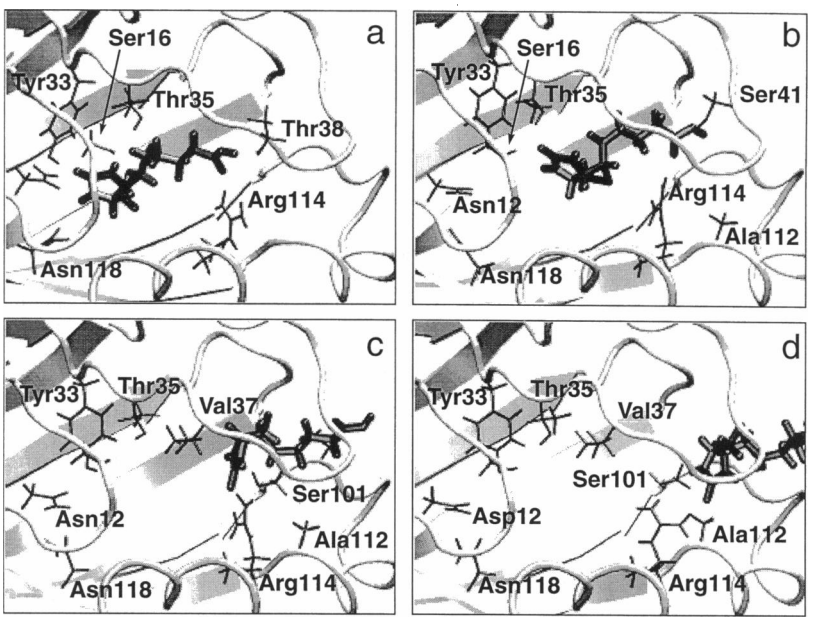

FIGURE 7 Contacts of biotin with polar residues in the process of unbinding. (*a*) $t = 0$ ps; head contacts: Tyr33, Ser16, Asn118, Asn12; tail contacts: Arg114, Thr38. (*b*) $t = 195$ ps; head contacts: Ser16, Thr35, Val37 (not shown); tail contacts: Ser41, Arg114. (*c*) $t = 372$ ps, biotin leaves the binding site; head contacts: Arg114 (two hydrogen bonds), Ser101, Trp110 (weak; see Fig. 8 *c*); tail contacts: Ser102 (not shown). (*d*) $t = 495$ ps; head contacts: Arg114, Ala112, Ser101, Ser102 (not shown).

THEORETICAL CONSIDERATIONS

The dissociation of avidin and its biotin ligand, without external forces, involves activated barrier-crossing events. The bound state of biotin corresponds to the lowest free energy of the system. To unbind biotin, the substrate must overcome potential barriers separating the bound state and the dissociated state. If the energies that mediate the adhesion of biotin to avidin are comparable to thermal energies, i.e., to k_BT, potential barriers that separate the two states can be overcome by thermal fluctuations. The barrier crossing requires longer times for higher barriers.

Applied forces lower the barriers, as shown in Fig. 9 for the case of a constant force F and a sample potential $U(x)$ exhibiting a single barrier. The positions $x = a$ and $x = b$ in Fig. 9 correspond to the bound and the transition state of biotin. Lowering of the barrier decreases the time required for unbinding, until the unbinding actually occurs within a desired period. In fact, the rupture force is only well defined if one specifies the time allotted for unbinding to occur. One must ask what force is necessary to lower the barrier of unbinding sufficiently to overcome the latter on a certain time scale, e.g., within a millisecond.

In this section we consider schematic models for force-induced unbinding that allow us to interpret the simulation results reported above. We first consider unbinding induced by a constant force that does not change in time or space.

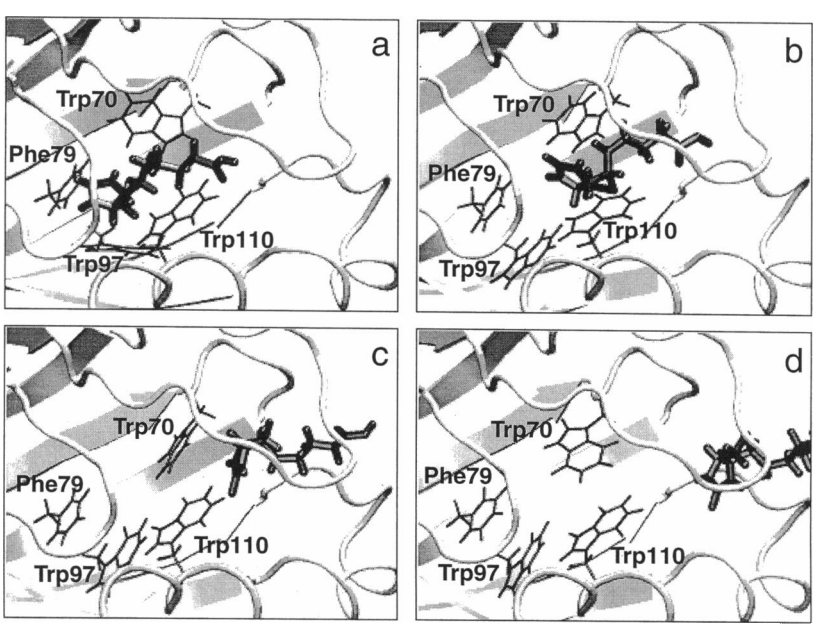

FIGURE 8 Contacts of biotin with nonpolar residues in the process of unbinding. (*a*) $t = 0$ ps; biotin is deeply buried inside the binding pocket. The head of biotin is in close contact with Phe79 and Trp97. Trp70 and Trp110 of the adjacent avidin monomer embrace biotin from the sides. (*b*) $t = 195$ ps; the head of biotin lost contact with Phe79 and Trp97 and moved closer to Trp70 and Trp110. (*c*) $t = 372$ ps; biotin left the binding site; a weak hydrogen bond is formed between Trp110 and O12 of biotin. (*d*) $t = 495$ ps; biotin is completely out of the binding pocket.

TABLE 1 Summary of polar contacts of biotin head along the rupture paths

$\alpha \times 10^3$ ps Å$^2/k_BT$	1	2	3	F/pN
100	Asn118 Asn12 Ser16 Thr35	Tyr33 Thr35		750
50	Asn118 Asn12 Ser16	Tyr33 Thr35 Val37	Thr35 Val37	775
20	Asn118 Asn12 Thr35 Val37	Ser16 Tyr33	Thr35 Val37	650
10	Asn118 Asn12 Ser16 Tyr33 Thr35 Val37 Phe72	Thr35 Val37 Phe72		700
8	Asn118 Asn12 Ser16 Thr35 Leu14	Tyr33 Leu14 Val37 Phe72	Thr35 Val37 Phe72	650
5	Asn118 Asn12 Ser16 Tyr33 Trp70 Leu99	Trp70 Leu99		450
4	Asn118 Asn12 Ser16 Tyr33 Thr77 Leu99 Trp97	Thr77 Leu99 Trp97		800
2	Tyr33 Asn12 Asn118 Thr35 Val37	Thr35 Ser16 Val37		450

This model can be used to illustrate the general characteristics of forced unbinding. We then introduce models involving space- and time-dependent forces.

Unbinding induced by a constant force

A constant force applied to unbind a ligand can lower key barriers along the ligand's pathway, as shown in Fig. 9. In this case one can determine the mean first passage time τ for the ligand to move from position $x = a$ to position $x = b$ and its dependence on the applied force. We pursue the question of how observation of τ reveals the properties of the unperturbed binding potential $U(x)$.

Langevin equation in the strong friction limit

We consider the unbinding of biotin from avidin to involve a single degree of freedom x. Because the time scale of unbinding is much longer than velocity relaxation, i.e., longer than about 1 ps, the so-called strong friction limit in which inertial effects are neglected can be safely adopted. In this limit the motion of biotin is governed by the Langevin equation

$$\gamma\dot{x} = -\frac{dU}{dx} + F + \sigma N(t). \tag{3}$$

Here x describes the length of the unbinding path; $U(x)$ the associated thermodynamic potential and F a force along the path; γ is the friction coefficient; $N(t)$ represents white noise of unit amplitude, i.e., with correlation function $\langle N(t + t_0)N(t_0)\rangle = \delta(t)$; and σ is the amplitude of the fluctuating forces described by $N(t)$ (Gardiner, 1985). According to the fluctuation-dissipation theorem, γ and σ are related through temperature as $\sigma^2/\gamma = 2k_BT$. Because the AFM experiment is carried out at constant temperature and pressure, the potential $U(x)$ should be identified with the Gibbs free energy G of the system. This implies that U, in general, is temperature dependent.

The probability distribution $p(x,t)$ of finding biotin at position x is governed by the Smoluchowski equation associated with the Langevin equation (Eq. 3):

$$\frac{\partial}{\partial t}p(x,t) = D\frac{\partial}{\partial x}\left[\beta\left(\frac{\partial U}{\partial x} - F\right) + \frac{\partial}{\partial x}\right]p(x,t). \tag{4}$$

where $\beta = 1/k_BT$, and $D = \sigma^2/2\gamma^2$ is the diffusion coefficient.

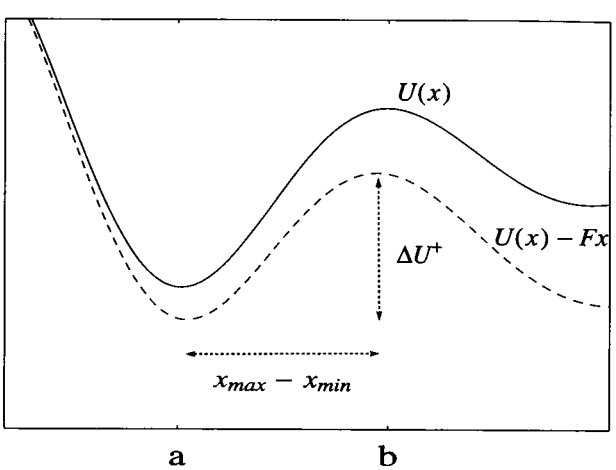

FIGURE 9 Schematic potentials $U(x)$, and $U(x) - Fx$.

Mean first passage time

To describe the rupture process we can study the mean first passage time $\tau(F)$ for the move of biotin from a, the minimum of the potential $U(x)$, to b, the maximum of $U(x)$, in Fig. 9. If the activation barrier in the path $a \rightarrow b$ is high compared to k_BT, the rate of crossing from a to b is very

small, but even when no force F is applied to biotin, the ligand eventually dissociates from avidin. The time $\tau(F)$ that follows from Eq. 4 is given by (Schulten et al., 1981; Gardiner, 1985)

$$\tau(F) = \frac{1}{D}\int_a^{b+} dy \exp[\beta(U(y) - Fy)]\int_{-\infty}^{y} dz \times \exp[-\beta(U(z) - Fz)], \quad (5)$$

where $b+ > b$ is a point in the vicinity of b. As a function of F, $\tau(F)$ is monotonously decreasing and concave, i.e., it satisfies

$$\frac{d\tau}{dF} = -\frac{\beta}{D}\int_a^{b+} dy \exp[\beta(U(y) - Fy)]\int_{-\infty}^{y} dz \times \exp[-\beta(U(z) - Fz)](y - z) < 0, \quad (6)$$

$$\frac{d^2\tau}{dF^2} = \frac{\beta^2}{D}\int_a^{b+} dy \exp[\beta(U(y) - Fy)]\int_{-\infty}^{y} dz \times \exp[-\beta(U(z) - Fz)](y - z)^2 > 0. \quad (7)$$

Therefore its inverse function $F(\tau)$ is a single-valued function of τ, and there is always a force F for a given unbinding time τ, e.g., for $\tau = 1$ ms.

Drift motion regime

In case of a large applied force $F - F_0(x) \gg k_BT/(b - a)$, where $F_0(x) = dU/dx$, Eq. 5 can be reduced to the expression

$$\tau(F) = \int_a^b dx \frac{\gamma}{F - F_0(x)}. \quad (8)$$

This is the solution of Eq. 3 when the fluctuating force is negligible. When F approaches $F_0(x)$ from above, the solution of the equation $F - F_0(x) = 0$ is reached at point x_{in}, the inflection point of the potential $U(x)$. For this force, i.e., for $F = F_0(x_{in})$, the unbinding time τ goes to infinity. This could bring one to the misleading conclusion that by increasing the time of extrusion of a ligand from the protein one can measure the maximum slope of the potential U between points a and b. However, this is not the case, because in the vicinity of x_{in} the condition $F - F_0(x) \gg k_BT/(b - a)$ is not valid. In fact, one can see from Eq. 5 that τ remains finite for all applied forces.

Activated events regime

In the opposite case, i.e., for $\beta[U(x) - Fx]$ being large at some point in the interval $[a, b]$, expression 5 can be reduced to the Kramers' relation:

$$\tau = \frac{2\pi\gamma}{\omega_{min}\omega_{max}} e^{\beta\Delta U^{\#}}, \quad (9)$$

where

$$\Delta U^{\#}(F) = U[(x_{max}(F)] - U[x_{min}(F)] - F(x_{max} - x_{min}). \quad (10)$$

$\Delta U^{\#}$ is the potential barrier that must be surmounted, $x_{min}(F)$ and $x_{max}(F)$ are the minimum and the maximum of $U(x) - Fx$ and $\omega^2_{min}, \omega^2_{max}$ are the absolute values of the curvatures of the potential at $x_{min}(F)$ and $x_{max}(F)$ (see Fig. 9). It is easy to show then (ignoring logarithmically small corrections) that the rate of unbinding, i.e., $k = \tau^{-1}$, satisfies

$$-\frac{\partial}{\partial F}\Delta U^{\#} = \frac{1}{\beta}\frac{\partial}{\partial F}\log k(F) = x_{max}(F) - x_{min}(F). \quad (11)$$

Reconstruction of $U(x)$ from rupture force

Probably the most important question about AFM experiments is the amount of information about the potential $U(x)$ that can be obtained by measuring the force dependence of the unbinding rate $k(F)$. In Kramers' approximation the expression $k_BT \log k(F)$ is formally analogous to the Legendre transform of $U(x)$. So we could expect to reconstruct the potential by taking the inverse Legendre transform of expression 10,

$$\Delta U(\Delta x) = -\frac{1}{\beta}\log k(F^*) + F^*\Delta x, \quad (12)$$

where we used Eq. 11, $\Delta x = x_{max} - x_{min}$, and F^* satisfies

$$\frac{1}{\beta}\frac{\partial}{\partial F}\log k(F^*) = \Delta x. \quad (13)$$

The function $\Delta U(\Delta x)$ obtained this way is not the potential function $U(x)$, but rather the maximum of the energy barrier that occurs between two points separated by a distance Δx,

$$\Delta U(\Delta x) = \sup_{x\in[a,b-\Delta x]} \{U(x + \Delta x) - U(x)\}. \quad (14)$$

$\Delta U(\Delta x)$ thus contains valuable information on the height and steepness of the energy barrier $U(x)$, i.e., it may reveal whether the activation energy is distributed evenly in $[a, b]$ or is localized in a short interval (as one could expect for highly specific biological interactions involving hydrogen bonding, etc.). This method cannot, however, provide the relative location of the energy barrier within $[a, b]$. Indeed, one can only reconstruct the convex hull of $U(x)$ from $k(F)$. Hence the amount of information about the thermodynamic potential $U(x)$ that can be obtained from rupture experiments is fairly limited.

Force-induced unbinding in the case of a sawtooth potential

To illustrate the above, we consider the simplest binding interaction described by a potential:

$$U(x) = \begin{cases} +\infty & \text{for } x < a, \\ \Delta U \dfrac{x-a}{b-a} & \text{for } a \le x \le b, \\ -\infty & \text{for } x > b. \end{cases} \quad (15)$$

In this case expression 5 can be integrated to yield

$$\tau(F) = 2\tau_d \delta(F)^{-2}[e^{\delta(F)} - \delta(F) - 1], \quad (16)$$

where $\tau_d = (b-a)^2/2D$ and

$$\delta(F) = \beta[\Delta U - F(b-a)]. \quad (17)$$

One can convince oneself that τ, as given by Eq. 16, is positive for all values of $\delta(F)$. We want to discuss this result in three regimes of the force values F.

Diffusive regime

In the so-called diffusive regime, characterized by forces F for which $\delta(F) \approx 0$, i.e., $F \approx \Delta U/(b-a)$ with an error of order $k_BT/(b-a)$, one obtains

$$\tau(F) = \tau_d\left(1 + \frac{\delta(F)}{3}\right). \quad (18)$$

In this regime the applied force counterbalances the internal binding force $-dU/dx$, so that biotin is subject to free diffusion; in this case the mean time needed to diffuse from a to b is indeed τ_d. Assuming for biotin an effective diffusion coefficient of 1 Å^2/ns, i.e., the diffusion coefficient of the heme group in myoglobin as determined from Mößbauer spectra (Nadler and Schulten, 1984), one expects an unbinding time of 25 ns for a binding pocket 7 Å in length.

Activated regime

For forces corresponding to positive δ and $e^{\delta(F)} \gg 1$, δ the mean time of unbinding is

$$\tau_{act} \approx 2\tau_d \delta(F)^{-2} e^{\delta(F)}, \quad (19)$$

which is equivalent to the Kramers' relation (Eq. 9). Obviously, in this case τ is very large. Assuming again that D = 1 Å^2/ns and $b - a$ = 7 Å, a δ value of 15.37 leads to unbinding within a millisecond. To carry this example further, a barrier of ΔU = 25 kcal/mol, similar to that of streptavidin (Chilcotti et al., 1995), and a rupture force of 155 pN, according to Eq. 17, would also imply δ = 15.37, i.e., unbinding within 1 ms. Such a δ-value corresponds to a barrier for unbinding, including the applied force, of 9 kcal/mol. We refer to this regime of force values as the regime of activated events. Apparently the AFM experiments with unbinding times of 1 ms are in this regime.

Drift regime

In the case of negative $\delta(F)$ values corresponding to $e^{\delta(F)} \ll 1 \ll |\delta(F)|$,

$$\tau_{diss} \approx 2\tau_d |\delta(F)|^{-1}. \quad (20)$$

This regime involves forces that are so strong that biotin undergoes a drift motion governed by Eq. 3 in the limit that the fluctuating force $\sigma N(t)$ is negligible compared to the applied force. In this case a δ value of -100 would lead to rupture within 500 ps, i.e., to biotin motion of 7 Å within this time. In the case where ΔU = 25 kcal/mol, D = 1 Å^2/ns, and $b - a$ = 7 Å, a force of about 800 pN would lead to rupture within 500 ps. This simple example illustrates that molecular dynamics simulations by necessity operate in a regime that is different from that of AFM experiments and that forces of several hundred piconewtons are required to complete the rupture. The scaling behavior of the drift regime, characterized by Eq. 20, differs qualitatively from the activated regime as characterized by Eq. 19. Hence one cannot expect that molecular dynamics simulations of rupture processes can be scaled toward the experimental force and time scales as stated by Grubmüller et al. (1996).

Unbinding induced by time-dependent forces

The results presented in the previous section are adequate to describe the forced unbinding process in a qualitative way. However, it is necessary to remove the restriction of a constant force to be able to make connection with AFM experiments and MD simulations, because the forces arising in the latter cases are time-dependent.

The forces applied by the AFM cantilever are essentially harmonic and have the form

$$F(x, t) = -f(x - vt), \quad (21)$$

where f is the spring constant and v is the velocity of the cantilever tip, assumed to be constant. Alternatively, one can hold the end of the spring fixed and increase the spring constant in time, as described by Eqs. 1 and 2. The spring constant f, related to the stiffness of the spring, is an important element in the interpretation of rupture forces, because it defines the equilibrium fluctuations of the ligand position δx. In the drift regime, i.e., when $F(x, t) > dU/dx$, the position fluctuations are $\delta x = (k_BT/f)^{1/2}$, and the applied force fluctuations are related to f through $\delta F = (k_BTf)^{1/2}$. In the case of AFM, the cantilever force constants measure 6 pN/Å (Moy et al., 1994a), which corresponds to $\delta x \approx 3$ Å and $\delta F \approx 15$ pN. These values imply that the ligand can fluctuate in a large area of the binding pocket during the unbinding process. In contrast, the spring employed in the simulations of Grubmüller et al. (1996) with f = 280 pN/Å corresponds to $\delta x \approx 0.4$ Å and $\delta F \approx 100$ pN. The position of the ligand is then constrained at any given time to a very small region of space, such that only local properties of the binding potential are sampled.

To compare scenarios corresponding to weak and stiff springs acting through a force in Eq. 21 as well as through a force in Eq. 1, we simulated a random process governed by the corresponding Langevin equation (Eq. 3), assuming the schematic binding potential (cf. Eq. 15):

$$U(x) = \begin{cases} 10F_0(a - x) & \text{for } x < a, \\ F_0(x - a) & \text{for } a \le x \le b, \\ 10F_0(b - x) + F_0(b - a) & \text{for } x > b. \end{cases} \quad (22)$$

where $F_0 \approx 250$ pN, which corresponds to a barrier $\Delta U =$ 25 kcal/mol and a linear potential energy ramp in the binding pocket of length 7 Å. The force of 10 F_0 at $x <$ areflects the ligand back into the pocket in the interval [a, b], whereas the same force at $x > b$ repels the ligand away from the binding pocket; we choose $b - a = 7$ Å.

The position $x(t)$ of the ligand was then evaluated at discrete time steps j dt, $j = 1, 2, 3\ldots$, using

$$x(t + \mathrm{d}t) = x(t) + \beta D \mathrm{d}t\left[-\frac{\mathrm{d}U}{\mathrm{d}x} + F(x, t)\right] + (2D\mathrm{d}t)^{1/2} r(t). \quad (23)$$

where $r(t)$ are normally distributed random numbers determined as described by Press et al. (1992) and where we chose d$t = 1$ ps. The ligand is initially located at $x(0) = 0$. We assume in all calculations a friction (see Eq. 3) of $\gamma =$ 2000 ps pN/Å.

Stiff cantilever

In the following we assume a stiff cantilever, choosing $f =$ 280 pN/Å and $v = 0.015$ Å/ps (Grubmüller et al., 1996) in Eq. 21. A typical Langevin trajectory for the model shown is presented in Fig. 10. The average force, amplitude of the fluctuations, and correlation time compare well with the simulations of Grubmüller et al. (1996). For the velocity assumed, the length of the binding pocket is traversed in about 500 ps. In fact, at this point in time the ligand becomes unbound, as seen in the sudden drop of the force

$$F(x, t) = -f[x(t) - a - vt] \quad (24)$$

presented in Fig. 10. The total force acting on the ligand in the interval [a, b] is $-f[x(t) - a - vt + F_0/f]$. This force is pointing into the pocket at $x = a$ until $vt > F_0/f$, i.e., until $t \approx 100$ ps. The frictional force γv measures 30 pN. For the spring to add this force, the end must move for another 10 ps. One can discern from Fig. 10 that the force increases on the average until $t = 110$ ps. After this time the average force measures about 250 pN + 30 pN = 280 pN, i.e., as much as the local gradient combined with the frictional force. This behavior reflects the fact that a stiff spring measures only local properties of $U(x)$, i.e., the slope of the potential.

For a further description one may consider solely the evolution of the average position $\langle x \rangle$, neglecting the effect of fluctuating forces. For $t < t_0 = F_0/fv$, the applied force is weaker than the binding force, and biotin, in this model, is pushed into the binding pocket, so that $\langle x(t) \rangle \approx a$. For $t > t_0$, on the other hand, $\langle x(t) \rangle$ is governed by

$$\gamma \frac{\mathrm{d}}{\mathrm{d}t} \langle \Delta x(t - t_0) \rangle = fv(t - t_0) - f\langle \Delta x(t - t_0) \rangle, \quad (25)$$

where $\Delta x = x - a$. The solution to this equation is

$$\langle \Delta x(t - t_0) \rangle = v(t - t_0) - \frac{v\gamma}{f}[1 - \exp(-f(t - t_0)/\gamma)]. \quad (26)$$

The force applied to biotin is

$$\langle F(t - t_0) \rangle = F_0 + v\gamma[1 - \exp(-f(t - t_0)/\gamma)], \quad (27)$$

such that after a time of $t_0 + \tau$, where the relaxation time is $\tau = \gamma/f \simeq 7$ ps, the system experiences an average force $v\gamma + F_0 = 280$ pN. The latter value agrees with the results shown in Fig. 10.

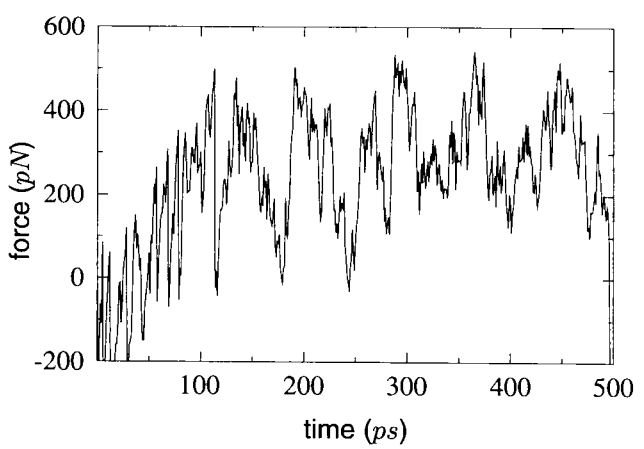

FIGURE 10 The time dependence of the applied force for a stiff cantilever $f = 280$ pN/Å, $v = 0.015$ Å/ps, and $\gamma = 2000$ pN ps/Å.

Soft cantilever

To model the behavior of a tip as used in an AFM experiment, we repeated the calculations described above, except for taking $f = 6$ pN/Å. The force

$$F(x, t) = -f[x(t) - a - vt] \quad (28)$$

resulting in this case is presented in Fig. 11 and differs strongly from the result shown in Fig. 10. The discrepancy arises because the total force $-f[x(t) - a - vt + F_0/f]$ does not become positive (i.e., outward pointing) until $t = 2800$ ps. To overcome the frictional force of 30 pN requires another 300 ps, and to pass 7 Å requires 500 ps more, so that the rupture can occur at $t \approx 3600$ ps. The longest relaxation time of a Brownian oscillator measures γ/f, which, in the present case, is about 300 ps. This adds an uncertainty to the rupture such that the 3700 ps instance of the rupture is

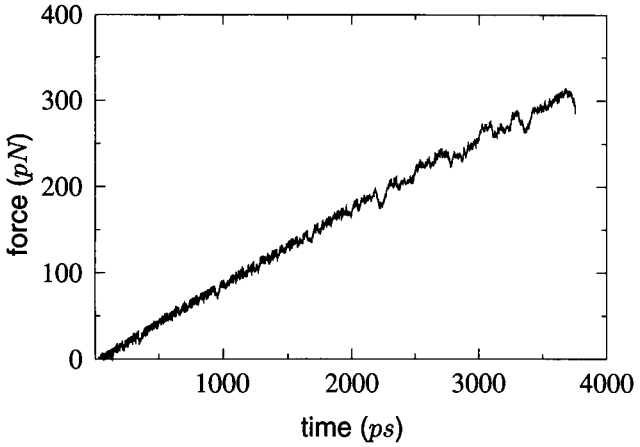

FIGURE 11 The time dependence of the applied force for a soft AFM-like cantilever $f = 6$ pN/Å, $v = 0.015$ Å/ps, and $\gamma = 2000$ pN ps/Å.

roughly in accordance with the simple description given. By the time rupture occurs, the spring has been overstretched, corresponding to a maximum force, the rupture force, of 310 pN.

Slowly stiffening cantilever

We have also modeled the unbinding when a spring with increasing force constant (cf. Eqs. 1 and 2), i.e., a slowly stiffening cantilever, is applied to the ligand. For this purpose we employ the force

$$F(x, t) = \alpha t[d - x(t)]. \tag{29}$$

with $d = 20$ Å and $\alpha = 0.004\ k_BT$/ps Å^2. The resulting $F[x(t), t]$ is presented in Fig. 12. The results are similar to the case of a weak cantilever, except that the rupture already occurs at about 150 ps with a maximum force of 400 pN.

We want to consider now the relationship between the slope F_0 and the maximum force F_r arising during the rupture process, i.e., the rupture force. The total force

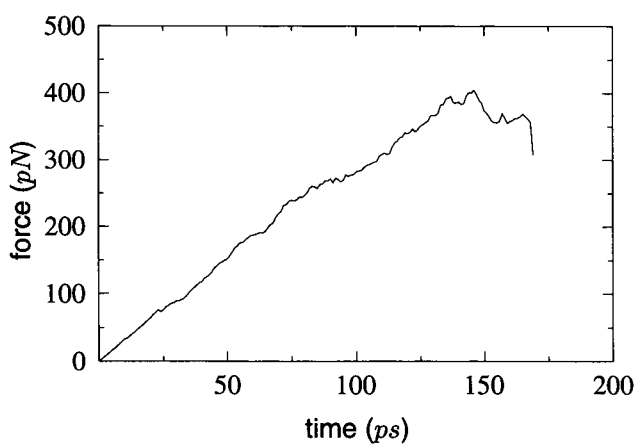

FIGURE 12 The time dependence of the applied force for a slowly stiffening cantilever $\alpha = 4 \times 10^{-3}\ k_BT$/ps Å^2, and $\gamma = 2000$ pN ps/Å.

$\alpha t[d - x(t) + F_0/\alpha t]$ becomes positive near $x = 0$ at $t_0 \approx 70$ ps, and the ligand starts to drift out of the pocket. The drift is governed by (cf. Eq. 3)

$$\gamma \dot{x} = \alpha(t - t_0)d, \tag{30}$$

the solution of which is

$$x(t) = x(t_0) + \frac{\alpha d}{2\gamma}(t - t_0)^2. \tag{31}$$

Rupture is completed at time t_r characterized through $x(t_r) - x(t_0) = b - a$, i.e., at time

$$t_r = t_0 + \left(\frac{2(b - a)\gamma}{\alpha d}\right)^{1/2}. \tag{32}$$

which is about 160 ps. This is, indeed, the time at which rupture is discernible in Fig. 12. The rupture force is $\alpha(d - 7$ Å$)$ 160 ps, i.e., 340 pN. This value agrees well with the force seen in Fig. 12 just before the rupture. The quality of this estimate underscores that the stiffening cantilever model, in fact, operates in the drift regime.

Distribution of rupture forces

We have demonstrated above (cf. Eqs. 5–7) that the rupture time of the ligand, expressed through the mean first passage time, is a unique function of an applied homogeneous force or, conversely, that a given rupture time corresponds to a unique force. We want to demonstrate now that in the case of time-dependent forces the observed rupture force, defined as the force applied at the moment of unbinding, becomes a random variable and exhibits a distribution that can be estimated (Evans and Ritchie, 1996). We assume that the applied force is weak, such that rupture times are longer than diffusional relaxation times. One can assume then that the ligand is always in a quasi-equilibrium state and that, within the binding pocket, the dependence of the applied force $F(x, t)$ on x can be neglected if the cantilever is soft enough. In this case the number of bound ligands obeys the first-order kinetics:

$$\dot{n}_b = -k[F(t)]n_b, \tag{33}$$

where $n_b(t)$ is the fraction of particles bound at time t and $k[F(t)]$ is the rate constant of unbinding when the force is $F(t)$. Equation 33 can be integrated to yield

$$n_b(t) = e^{-\int_0^t dt' k[F(t')]}. \tag{34}$$

We assume in the remainder of this section that the rate $\dot{F}$ of the change of force is constant and positive. One can then replace time everywhere by F. Using

$$\frac{dn_u}{dF} = \frac{1}{\dot{F}}\frac{dn_u}{dt} = -\frac{1}{\dot{F}}\dot{n}_b(t), \tag{35}$$

where $n_u(t)$ is the number of particles already unbound at

time t and $n_u = 1 - n_b$, Eq. 33 can be rewritten as

$$\frac{dn_u}{dF} = \frac{k(F)}{\dot{F}} n_b(F). \tag{36}$$

$k(F)$ can be related to the mean first passage time $\tau_{act}(F)$ ($k(F) = 1/\tau_{act}(F)$), which is furnished by Eq. 19. Accordingly, the rate constant is

$$k(F) = k_d(F)e^{-\delta(F)}, \tag{37}$$

where $k_d(F) = \delta(F)^2/2\tau_d$, and $\delta(F)$ is given by Eq. 17.

The probability $p(F)$ that a particle will unbind with the applied force F is dn_u/dF. This probability can be expressed through the r.h.s. of Eq. 36 and further evaluated. In the case of a linear potential (Eq. 15) one obtains, using Eqs. 34 and 37,

$$p(F) = \frac{k_d(F)}{\dot{F}} \exp\left\{-\delta(F) - \frac{1}{\dot{F}}\int_0^F dF' k_d(F') e^{-\delta(F')}\right\}. \tag{38}$$

$k_d(F)$ appearing in this expression is a slowly varying function of F, which will be assumed to be constant. The integral arising in Eq. 38 can then be readily evaluated

$$\frac{k_d}{\dot{F}}\int_0^F dF' e^{-\beta[\Delta U - F(b-a)]} = \frac{k_d}{\beta\dot{F}(b-a)} e^{-\beta\Delta U}(e^{\beta F(B-a)} - 1). \tag{39}$$

Substituting Eqs. 17 and 39 into Eq. 38 yields

$$p(F) = \frac{k_d}{\dot{F}} \exp\left\{\beta(F - F_0)\Delta x - \frac{k_d}{\beta\Delta x\dot{F}}(e^{\beta(F-F_0)\Delta x} - e^{-\beta F_0 \Delta x})\right\}, \tag{40}$$

where $F_0 = \Delta U/\Delta x$, and $\Delta x = b - a$.

The resulting probability distribution is shown schematically in Fig. 13 and is seen to exhibit a bell-shaped form with a pronounced maximum at F^*. The maximum is characterized through

$$\beta(F^* - F_0)\Delta x = \log\left(\frac{\beta\dot{F}\Delta x}{k_d}\right). \tag{41}$$

The width δF of $p(F)$ is determined by the second derivative of the exponential in Eq. 40, given by $\delta F = k_B T/\Delta x$. This expression can be interpreted as the average force produced by thermal fluctuations within a binding pocket of size Δx.

In case where the potential $U(x)$ exhibits a pronounced barrier, rather than being of linear form, one can employ Kramers' relation (Eq. 9) and obtain from Eq. 36 similarly for the distribution of rupture forces,

$$p(F) = \frac{\omega_{min}\omega_{max}}{2\pi\gamma\dot{F}} \exp\left(-\beta\Delta U^{\#}(F) - \int_0^{t(F)} dt' k(F(t'))\right). \tag{42}$$

This distribution also exhibits a pronounced maximum at F^*, given by the extremum condition derived from the r.h.s. of Eq. 42,

$$-\beta\frac{\partial}{\partial F}\Delta U^{\#} - k(F)\frac{dt}{dF} = 0. \tag{43}$$

If one ignores the force dependence of the prefactors in Kramers' relation, one obtains, using Eqs. 10 and 11, for the width of the distribution for a general potential $U(x)$: $\delta F = k_B T/\Delta x(F^*)$, where $\Delta x(F^*) = x_{max}(F^*) - x_{min}(F^*)$.

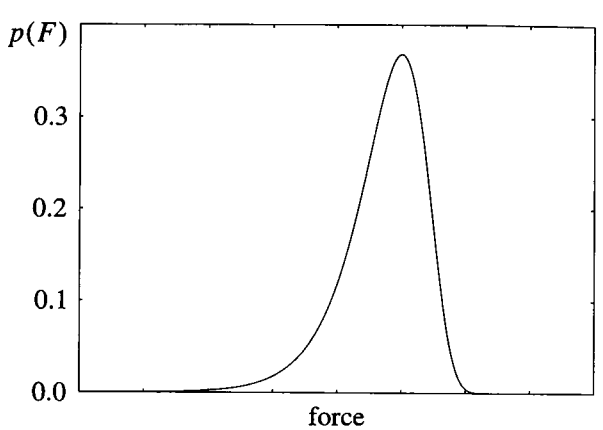

FIGURE 13 The distribution of the rate of unbinding as a function of the applied force.

DISCUSSION

In this paper we investigated the pathways of forced unbinding of avidin and biotin. The simulations were inspired by AFM measurements of the process (Florin et al., 1994; Moy et al., 1994b), but the approach promises to be of wider significance than proving consistency of molecular dynamics simulations with AFM data. In fact, in this respect the present paper produces a negative result, in that the claim by Grubmüller et al. (1996) that simulations can reproduce observed rupture forces quantitatively has not been substantiated. We attribute this mainly to the fact that in the simulations of these authors, only a streptavidin monomer has been simulated, in which case one side of the binding pocket, usually covered by Trp120 of another streptavidin monomer, is left open. Because the authors also solvated their system in water, it is likely that biotin was actually solvated to a significant degree in the binding pocket, weakening the adhesion forces to a degree that rupture forces below 200 pN were found, whereas the present simulation with an intact binding pocket yielded much larger values.

In fact, we suggest that the six order of magnitude gap in the time scales of AFM measurements and simulations cannot be readily bridged. Nevertheless, the simulations of enforced unbinding of biotin from avidin revealed an interesting scenario of stepwise slips involving changes of both protein-ligand hydrogen bond patterns and hydrophobic

contacts, as well as a barrier imposed by a protein loop capping the binding pocket. These phenomena are thought provoking and may characterize the actual process of unbinding.

One might criticize our simulations for the lack of inclusion of water. It is certainly desirable to include water in future simulations. However, we would expect that the actual binding pocket is not affected by the presence of water. In fact, AFM experiments established a linear correlation of the adhesion force with the unbinding enthalpy and not the free energy of the system (Moy et al., 1994b). Therefore, the change of entropy during the process of unbinding is negligible, and entropy-driven processes such as solvation effects occur beyond the rupture point.

The main conclusion of this study is that a new methodology has emerged for exploring ligand binding and unbinding, and ligand-protein recognition or DNA sequence recognition by regulatory proteins. The mechanical manipulation methods applied can also play an important role in structure building and docking. The paper addresses the issue of how manipulation by means of soft or stiff harmonic forces, and using different speeds of pulling or increasing forces yield different types of information, e.g., local or more global features of potentials. The approach reverses the previous aim of thermodynamic perturbation theory, which seeks to determine differences in thermodynamic potentials through extremely slow manipulation, in that irreversible contributions arising in the present approach are accepted and one seeks to identify them. In as much as irreversible processes accompany any nonequilibrium reactions, particularly the breaking of adhesive linkages in biological cells, the approach taken can yield crucial information.

Mechanical manipulations of the type investigated in this study are very timely because of recent developments in computational algorithms and hardware that bring interactive modeling of biopolymers within the reach of routine modeling work (Nelson et al., 1995, 1996; Humphrey et al., 1996). Naturally, investigators want to apply very rapid methods to realize true interactivity, but this will necessarily involve irreversibility of processes. Investigators will also seek suitable analysis methods that monitor the progress and nature of enforced reactions.

The value of the approach is best demonstrated by summarizing the information revealed on the unbinding of biotin. We have found that the unbinding is a multistep process, each step corresponding to the rupture of a network of hydrogen bonds, which biotin forms with the polar residues in the binding pocket. The most significant bonds are formed between the head of biotin and Asn12, Ser16, Tyr33 as well as Thr35. As in streptavidin, the presence of aromatic residues Phe79, Trp97, Trp70, and especially Trp110 contributes significantly to the binding of biotin to avidin. The optimized "capping" interaction of Trp110 with the aliphatic chain of biotin has a large effect on the biotin-avidin binding enthalpy and accessibility of water to the binding pocket; the mutation of the analogous Trp120 in streptavidin to phenylalanine results in a 70-fold increase in the dissociation rate relative to wild-type streptavidin (Chilcotti and Stayton, 1995).

Futhermore, our simulations revealed the significance of flapping motions of the 3-4 loop of the avidin monomer. This loop is tightly closed on top of biotin's binding pocket, making its escape from the pocket virtually impossible. The fluctuation time for this loop as well as the relaxation time for many of the processes in the proteins is on the order of hundreds of nanoseconds. The loop will have enough time to open under experimental conditions, whereas during molecular dynamics simulations these fluctuation times are too long and the loop stays closed. In fact, during the simulated extrusion biotin hits the loop and remains caught by the loop until the external force increases sufficiently to fling the loop open, unless the loop is open artificially beforehand, as described in the Method section.

The methods developed here have already been employed beyond the avidin-biotin systems. Recently we used the method to identify the path of binding and unbinding of retinal in bacteriorhodopsin, and sequence-specific and sequence-nonspecific binding of nuclear hormone receptors to DNA, and to investigate a putative backdoor mechanism for P_i (inorganic phosphate) release after hydrolysis from ADP in actin. In the near future, interactive mechanical manipulations may play the same major role in biological modeling as thermodynamic perturbation theory.

The work reported identified various methodological challenges. A key open problem is the extension of the time scale to advance manipulation methods into the thermally activated regime, where agreement with observations can be expected. Another open problem is to identify and discount irreversible contributions to reveal the thermodynamic potentials underlying the motions of ligands in proteins. Computational techniques must also be vastly accelerated to make interactive molecular dynamics truly routine.

The authors are grateful to S. Bezrukov, E. Evans, D. Leckband, V. A. Parsegian, and Ch. Pidgeon for helpful suggestions. They also thank A. Balaeff, A. Dalke, I. Hofacker, and W. Wriggers.

This work was supported by grants from the National Institutes of Health (PHS 5 P41 RR05969-04), the National Science Foundation (BIR-9318159, DMR-93-14938), and the Roy J. Carver Charitable Trust.

REFERENCES

Balgi, G., D. E. Leckband, and J. M. Nitsche. 1995. Transport effects on the kinetics of protein-surface binding. *Biophys. J.* 68:2251–2260.

Baljon, R. C. A., and M. O. Robbins. 1996. Energy dissipation during rupture of adhesive bonds. *Science.* 271:482–484.

Bayer, E. A., and M. Wilcheck. 1980. The use of avidin-biotin complex as a tool in molecular biology. *Methods Biochem. Anal.* 26:1–45.

Bernstein, F. C., T. F. Koetzle, G. J. F. Meyer, M. D. Brice, J. R. Rogers, O. Kennard, T. Shimanouchi, and M. Tasumi. 1977. The protein data bank: a computer-based archival file for macromolecular structures. *J. Mol. Biol.* 112:535–542.

Binning, G., C. F. Quate, and G. Gerber. 1986. Atomic force microscope. *Phys. Rev. Lett.* 56:930–933.

Block, S., and K. Svoboda. 1994. Biological applications of optical forces. *Annu. Rev. Biophys. Biomol. Struct.* 23:247–285.

Brooks, B. R., R. E. Bruccoleri, B. D. Olafson, D. J. States, S. Swaminathan, and M. Karplus. 1983. CHARMm: a program for macromolecular energy, minimization, and dynamics calculations. *J. Comp. Chem.* 4:187–217.

Brünger, A. T. 1992. X-PLOR, Version 3.1: A System for X-ray Crystallography and NMR. The Howard Hughes Medical Institute and Department of Molecular Biophysics and Biochemistry, Yale University.

Chilcotti, A., T. Boland, B. D. Ratner, and P. S. Stayton. 1995. The relationship between ligand-binding thermodynamics and protein-ligand interaction forces measured by atomic force microscopy. *Biophys. J.* 69:2125–2130.

Chilcotti, A., and P. S. Stayton. 1995. Molecular origins of the slow streptavidin-biotin dissociation kinetics. *J. Am. Chem. Soc.* 117: 10622–10628.

Conn, P. M., editor. 1993. Receptors: Molecular Biology, Receptor Subclasses, Localization, and Ligand Design. Academic Press, San Diego, CA.

Evans, E., D. Berk, and A. Leung. 1991. Detachment of agglutinin-bonded red blood cells. *Biophys. J.* 59:838–848.

Evans, E., and K. Ritchie. 1997. Dynamic strength of molecular adhesion bonds. *Biophys. J.* 72:1541–1555.

Evans, E., K. Ritchie, and R. Merkel. 1995. Sensitive force technique to probe molecular adhesion and structural linkages at biological interfaces. *Biophys. J.* 68:2580–2587.

Florin, E.-L., V. T. Moy, and H. E. Gaub. 1994. Adhesion force between individual ligand-receptor pairs. *Science.* 264:415–417.

Frisch, M. J., G. W. Trucks, H. B. Schlegel, P. M. W. Gill, B. G. Johnson, M. A. Robb, J. R. Cheeseman, T. Keith, G. A. Petersson, J. A. Montgomery, K. Raghavachari, M. A. Al-Laham, V. G. Zakrzewski, J. V. Ortiz, J. B. Foresman, C. Y. Peng, P. Y. Ayala, W. Chen, M. W. Wong, J. L. Andres, E. S. Replogle, R. Gomperts, R. L. Martin, D. J. Fox, J. S. Binkley, D. J. Defrees, J. Baker, J. P. Stewart, M. Head-Gordon, C. Gonzalez, and J. A. Pople. 1995. Gaussian 94, Revision B.3. Gaussian Inc., Pittsburgh, PA.

Gardiner, C. W. 1985. Handbook of Stochastic Methods for Physics, Chemistry, and the Natural Sciences. Springer Verlag, New York.

Green, N. M. 1975. Avidin. *Adv. Protein Chem.* 29:85–133.

Green, N. M. 1990. Avidin and streptavidin. *Methods Enzymol.* 184: 51–67.

Grubmüller, H., B. Heymann, and P. Tavan. 1996. Ligand binding and molecular mechanics calculation of the streptavidin-biotin rupture force. *Science.* 271:997–999.

Heney, G., and G. A. Orr. 1981. The purification of avidin and its derivatives on 2-immunobiotin-6-aminohexylsepharose 4b. *Anal. Biochem.* 114:92–96.

Humphrey, W. F., A. Dalke, and K. Schulten. 1996. VMD—visual molecular dynamics. *J. Mol. Graphics.* 14:33–38.

Israelachvili, J. N., editor. 1992. Intermolecular and Surface Forces. Academic Press, London.

Kanzaki, M., and A. Iwasawa. 1995. A sensitive, non-isotopic immunoassay for progesterone using the avidin-biotin system. *Biomed. Res.* 16: 381–386.

Kuby, S. A. 1991. Enzyme Catalysis, Kinetics, and Substrate Binding. Study of Enzymes, vol. 1. CRC Press, Boca Raton, FL.

Leckband, D. E., F. J. Schmitt, J. N. Israelachvili, and W. Knoll. 1994. Direct force measurements of specific and nonspecific protein interactions. *Biochemistry.* 33:4611–4624.

Livnah, O., E. A. Bayer, M. Wilchek, and J. L. Sussman. 1993. Three-dimensional structures of avidin and the avidin-biotin complex. *Biochemistry.* 90:5076–5080.

McCammon, J. A., and S. C. Harvey. 1987. Dynamics of Proteins and Nucleic Acids. Cambridge University Press, Cambridge.

Miyamoto, S., and P. A. Kollman. 1993. Absolute and relative binding free energy calculations of the interaction of biotin and its analogs with streptavidin using molecular dynamics/free energy perturbation approaches. *Proteins Struct. Funct. Genet.* 16:226–245.

Moy, V. T., E.-L. Florin, and H. E. Gaub. 1994a. Adhesive forces between ligand and receptor measured by AFM. *Colloids Surfaces.* 93:343–348.

Moy, V. T., E.-L. Florin, and H. E. Gaub. 1994b. Intermolecular forces and energies between ligands and receptors. *Science.* 266:257–259.

MSI. 1994. QUANTA 4.0. Molecular Simulations, Burlington, MA.

Nadler, W., and K. Schulten. 1984. Theory of Mössbauer spectra of proteins fluctuating between conformational substates. *Proc. Natl. Acad. Sci. USA.* 81:5719–5723.

Nadler, W., and K. Schulten. 1985. Generalized moment expansion for Brownian relaxation processes. *J. Chem. Phys.* 82:151–160.

Nelson, M., W. Humphrey, A. Gursoy, A. Dalke, L. Kalé, R. D. Skeel, and K. Schulten. 1996. NAMD–a parallel, object-oriented molecular dynamics program. *J. Supercomput. Appl.* 10:251–268.

Nelson, M., W. Humphrey, A. Gursoy, A. Dalke, L. Kalé, R. Skeel, K. Schulten, and R. Kufrin. 1995. MDScope—a visual computing environment for structural biology. *Comput. Phys. Commun.* 91:111–134.

Press, W. H., S. A. Teukolsky, W. T. Vetterling, and B. P. Flannery. 1992. Numerical Recipes in C, 2nd Ed. Cambridge University Press, New York.

Pugliese, L., A. Coda, M. Malcovati, and M. Bolognesi. 1993. Three-dimensional structure of the tetragonal crystal form of egg-white avidin in its functional complex with biotin at 2.7 Å resolution. *J. Mol. Biol.* 231:698–710.

Pugliese, L., A. Coda, M. Malcovati, and M. Bolognesi. 1994. Crystal structure of apo-avidin from hen egg-white. *J. Mol. Biol.* 235:42–46.

Schulten, K., Z. Schulten, and A. Szabo. 1981. Dynamics of reactions involving diffusive barrier crossing. *J. Chem. Phys.* 74:4426–4432.

Schwabe, J. W. R., L. C. Chapman, J. T. Finch, D. Rhodes, and D. Neuhaus. 1993. DNA recognition by the estrogen receptor: from solution to the crystal. *Structure.* 15:187–204.

Suurkusk, J., and I. Wadso. 1972. Thermochemistry of the avidin-biotin reaction. *Eur. J. Biochem.* 28:438–441.

Svoboda, K., and S. M. Block. 1994. Force and velocity measured for single kinesin molecules. *Cell.* 77:773–784.

Swamy, M. J. 1995. Thermodynamic analysis of biotin binding to avidin. A high sensitivity titration calorimetric study. *Biochemistry.* 36: 219–225.

Wang, N., J. P. Butler, and D. E. Ingber. 1993. Mechanotransduction across the cell surface and through the cytoskeleton. *Science.* 260: 1124–1127.

Wilcheck, M., and E. A. Bayer. 1989. Avidin-biotin technology ten years on: has it lived up to its expectation? *Trends Biochem. Sci.* 14:408–412.

Zhang, L., and J. Hermans. 1996. Hydrophilicity of cavities in proteins. *Proteins Struct. Funct. Genet.* 24:433–438.